ISSN (Print) 1226-1750
ISSN (Online) 2233-6656
Journal of Magnetics 25(4), 601-605 (2020) https://doi.org/10.4283/JMAG.2020.25.4.601

Indirect Photon-counting Detector (PCD) for Transmission Imaging

Daehong Kim[1], Hakjae Lee[2], and Seung-Jae Lee[3,4]*

[1]*Department of Radiological Science, Eulji University, Seongnam 13135, Republic of Korea*
[2]*ARALE laboratory, Inc., Seoul, 02843, Republic of Korea*
[3]*Department of Radiological Science, Dongseo University, Busan 47011, Republic of Korea*
[4]*Center for Radiological Environment & Health Science, Dongseo University, Busan 47011, Republic of Korea*

(Received 22 October 2020, Received in final form 30 November 2020, Accepted 1 December 2020)

Photon-counting detectors (PCDs) are replacing energy integrating detectors in electromagnetic wave transmission imaging to achieve high performance. The purpose of this study was to develop an indirect PCD system for transmission imaging. The detector module is a combination of scintillator and SiPM, the SiPM is insensitive to magnetic field and operating at low voltage. A 2D array of a GAGG coupled with SiPM, positioning logic circuit, and preamplifier were enclosed in housing that sealed from light. A channel reduction circuit was used to identify the channel from the positioning logic circuit, and then output an analog pulse signal corresponding to the valid channel. The pulse signal measurements were performed using a oscilloscope. The profile analysis of the flood map confirmed that each point was distinct in both the center and peripheral regions. Additionally, the letters engraved on the phantom in the images were confirmed. Therefore, the indirect PCD system has potential for transmission imaging. Our future work will design an indirect PCD for low-energy photon detection and multi-energy imaging.

Keywords : PCD, electromagnetic wave, magnetic field, transmission imaging

1. Introduction

Medical diagnostic devices provide anatomical and functional information. In radiology, X-ray machines such as digital radiography (DR), computed tomography (CT), and mammography, which mainly display the structure of the human body, have been widely used. The trend toward high performance and qualitative improvements continue for detectors in X-ray imaging systems, such as replacing an energy integrating detector (EID) with a photon-counting detector (PCD).

Conventional X-ray imaging systems have been operated with EIDs. However, because the EID integrates signals of X-ray photons, the detector signal loses the energy information of individual photons. Additionally, an EID adds electronic noise [1].

Recently, energy resolved PCDs have been developed for X-ray imaging [2, 3]. A PCD counts the number of individual photons that exceed a preset threshold. For a given photon, the pulse height of the signal created by the deposited charge at the detector is proportional to the energy of the photon [4]. PCDs commonly use a direct conversion method for photon detection that does not require a scintillator. Semiconductors such as CZT and CdTe directly convert photons into electron hole pairs. When a bias voltage is applied to the semiconductor, electrons are collected by the anode to generate electron signals [5]. PCDs have some merits as a radiation detector. A PCD can reduce electronic noise by counting only signals that exceed the preset threshold. The PCD also gives the same weight factor to low-energy photons, which can increase the image contrast. Additionally, it is possible to reduce beam-hardening and obtain multi-energy images through energy bin settings [6]. However, the semiconductor has a low detection efficiency, it is difficult to fabricate large sizes, and the maintenance is expensive [7].

In our previous work, an indirect PCD was developed and the energy resolution was evaluated using a cerium-doped $Gd_3Al_2Ga_3O_{12}$ (GAGG) scintillator [8]. The indirect PCD was only designed to measure the photon spectrum. In this study, we developed an indirect PCD using GAGG and a silicon photomultiplier (SiPM) for 2D imaging.

*Corresponding author: Tel: +82-51-320-2719
Fax: +82-51-320-2958, e-mail: sjlee@gdsu.dongseo.ac.kr

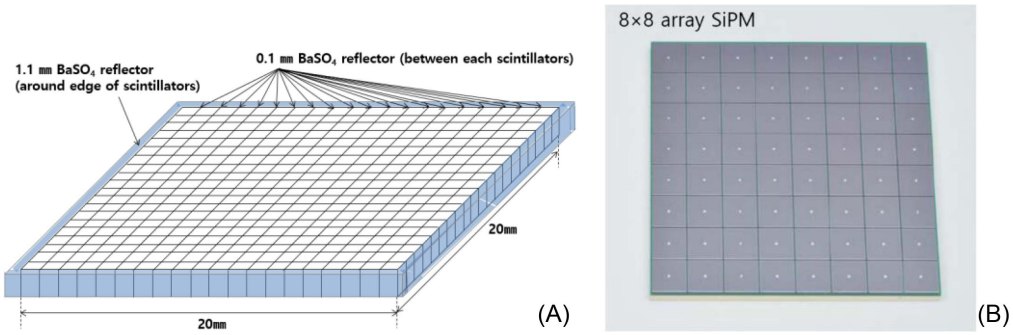

Fig. 1. (Color online) (A) is a 20 × 20 2D array GAGG scintillator with a $BaSO_4$ reflector. (B) is a 8 × 8 SiPM array.

GAGG crystals have a high stopping power, fast response, and high photon yield. The feature of SiPM is insensitive to magnetic field and operating at low voltage [7]. To obtain a phantom image, the pixelated GAGG crystal was coupled to a SiPM array, and a positioning logic circuit was also added. Therefore, the purpose of this study was to develop an indirect PCD system for transmission imaging.

2. Materials and Methods

2.1. 2D array of the GAGG scintillator and SiPM

We designed a 2D array of a GAGG scintillator coupled to a 2D array of SiPM for 2D transmission imaging. As shown in Fig. 1(A), the GAGG scintillator has a 20 × 20 array, pixelated with 0.9 × 0.9 × 3.5 mm^3 elements and a pixel pitch of 1 × 1 mm^2. The separator gaps between the scintillators were filled with 0.1 mm $BaSO_4$ reflective powder to increase light collection efficiency. The $BaSO_4$ powder was also wrapped around the scintillator array. Figure 1(B) shows a 8 × 8 SiPM array (MPPC®, Hamamatsu, Japan). The SiPM has a size of 24 × 24 mm^2, a pixel pitch of 50 × 50 μm^2, and a geometrical fill factor of 74 %.

2.2. Indirect photon-counting detector

The indirect PCD, which consists of a detector array, positioning logic circuit, preamplifier, and power supply, was developed as shown in Fig. 2. Electromagnetic waves are first converted into visible light through the GAGG crystal, which is converted further into the SiPM. The SiPM converts the visible light into an electrical signal. The active base consists of a positioning logic circuit and preamplifier. Signals from the SiPM can be read using a preamplifier. The signals are then fed to the positioning logic circuit, known as Anger Logic.

Since the PCD developed in this study differs in the number of pixels of the scintillator and the number of pixels of SiPM, the position of the light signal emitted from each scintillator was determined using the Anger Logic algorithm. The Anger Logic determines the X-Y position of each scintillation event as it occurs by using the weighted average of the SiPM signals. The X-Y position of the scintillator pulse is defined by Eqs. (1) and (2) [9]:

$$X_{position} = \frac{X_+ - X_-}{X_+ + X_-}, \quad (1)$$

Fig. 2. (Color online) Photograph of (a) the 2D array of GAGG scintillator coupled with the SiPM, (b) active base, (c) channel reduction circuit, and (d) power supply.

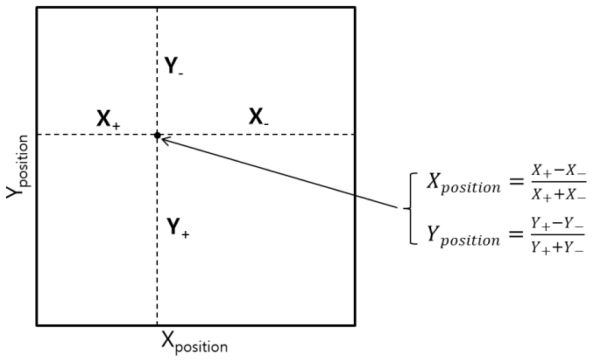

Fig. 3. Illustration of the position calculation with the Anger Logic algorithm. The X-Y position of each scintillation event using the weighted average of the SiPM signals.

$$Y_{position} = \frac{Y_+ - Y_-}{Y_+ + Y_-}. \quad (2)$$

The output of each SiPM is shared between four outputs (X_+, Y_-, Y_+, Y_-) using resistors. As shown in Fig. 3, X_+, X_-, Y_+, and Y_- are defined in one pixel of the SiPM sensor. The X-Y position of the light detected in the SiPM is calculated using Eqs. (1) and (2). Then, the position of X-Y is the position where the electromagnetic wave and the scintillator react.

In this study, since a 8 × 8 SiPM array was used, signals are measured in 16 channels. However, the pulse signal measurements were performed using a four channel oscilloscope (5 series MSO, Tektronix Inc., OR). Therefore, we used the channel reduction circuit to reduce the number of channels being digitized. In this study, the number of readout channels is reduced from 16 to 4.

The power supply applies a bias voltage to the radiation detector system. The bias voltage of SiPM is up to 80 V.

2.3. Indirect PCD system and experimental set-up

Figure 4(A) is the schematic diagram of the indirect PCD system, and Fig. 4(B) is a photograph of the indirect PCD system. As shown in Fig. 4(A), the 2D array of the GAGG coupled with SiPM, positioning logic circuit, and preamplifier were enclosed in a housing that was sealed from light. The channel reduction circuit is used to identify the channel from the positioning logic circuit. The channel reduction circuit then outputs an analog pulse signal corresponding to the valid channel. The pulse signal measurements were performed using a 4 channel oscilloscope.

Fig. 5. (Color online) ^{137}Cs source, phantom, and PCD for transmission imaging in a housing sealed from light.

Figure 5 illustrates a radioactive ^{137}Cs source, a phantom, and PCD for transmission imaging. The ^{137}Cs source emits a single gamma-ray of 662 keV, and their radioactivity is 8.946 μCi. The phantom is made of tungsten material with a size of 40 × 20 × 3 mm^3. The initials E and J are engraved on the phantom. Self-produced software for signal processing was used to obtain a flood map and phantom image. A scan time for the phantom is 8,491 seconds.

3. Results and Dicussion

This study is the preliminary results of an indirect PCD

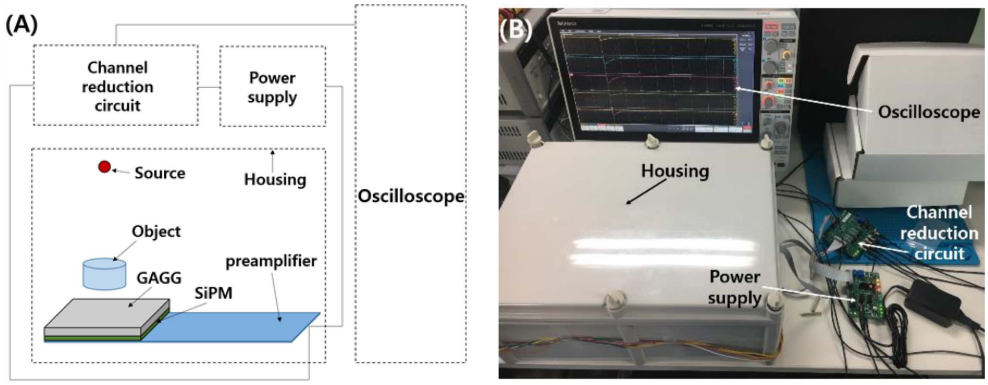

Fig. 4. (Color online) (A) The schematic diagram of indirect PCD system and (B) their picture.

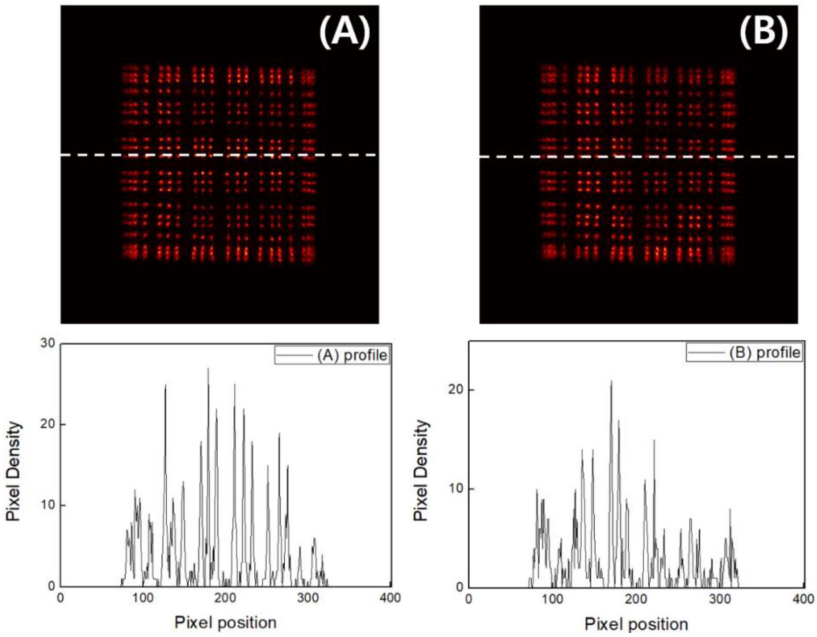

Fig. 6. (Color online) The flood map and profile for (A) E and (B) J acquired with the uniform source of ^{137}Cs. Each point in the image represents a crystal element.

system for transmission imaging. The characteristics of the indirect PCD with GAGG coupled to SiPM were performed in our previous work [8]. The results showed that GAGG has improved energy resolution than that of CsI and LYSO scintillators. Also, GAGG has a high material density and high light yield. Based on the results, we developed a 2D pixelated array imaging module system by adding a positioning logic circuit, such as Anger Logic, for signal processing of each pixel. We evaluated an indirect PCD system performance with GAGG and SiPM, and experimentally implemented 2D image acquisition using the indirect PCD system.

Experiments were performed to obtain the flood map, and then 2D image was generated from the flood map. Because the phantom is larger than that of the PCD, the flood maps for E and J was acquired, respectively. The number of 10^5 gamma rays was detected in each of the four channels of the oscilloscope. The four channel pulse signals from the oscilloscope were handled and analyzed by self-produced software. The flood map was generated by the information counted by location by applying Anger Logic to the channel energy value of 10^5 photons measured on each of the four channels.

Figures 6(A) and (B) show both the flood map and profiles of the flood map for the phantom characters E and J, respectively. The indirect PCD module is a 20 × 20 array of 20 × 20 GAGG crystals. As shown in Fig. 6, individual GAGG pixel can be identified in the flood map. In addition, the electronic readout provides low background noise and clear pixels identification in flood map for E and J, respectively. The profile analysis of the flood map for E and J confirmed that each point was distinct in both the center and peripheral regions. Generally, profile of the flood map is clearly visible [10]. However, in this study, since the flood map of the phantom image was acquired, the peak and valley uniformity of the profile was reduced.

The developed indirect PCD system was based on transmission image acquisition, which required the acquisition of phantom images to explore the potential as an imaging device. The phantom images were obtained from the results of the flood map as depicted in Figs. 7(A) and (B). In this experiment, the phantom images were acquired in counting mode and the energy bin was not set because the source was a single 662 keV energy source. The

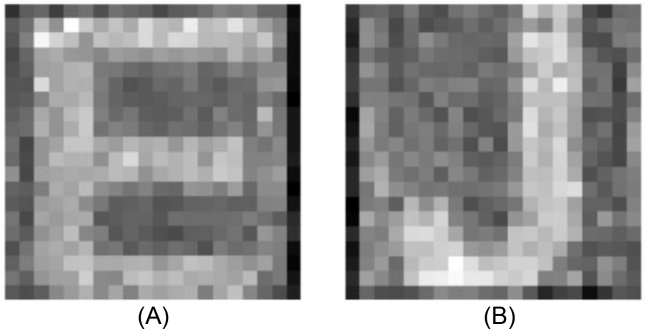

Fig. 7. The phantom images of (A) E and (B) J.

image results confirm that the shapes of E and J were observed. However, image quality such as contrast and high sharpness could be improved using low energy source. High-energy source increase the probability of Compton scattering, resulting in reducing contrast and image blurring. In diagnostic imaging, X-ray was used as a radiation source. Therefore, it is necessary to improve image quality using a low energy source.

In aspect of scintillator thickness, CsI scintillators are widely used for low energy radiation detection and are approximately 500-μm thick. Our indirect PCD used 3.5 mm thick GAGG scintillator. It is suitable for high energy radiation detection, but not for low energy radiation detection. Because a GAGG crystal is denser than CsI, it is necessary to reduce the thickness of the GAGG scintillator to detect low energy radiation.

For phantom imaging, 10^5 photons were detected; however, clinical trials require high flux radiation exposure, such as 10^9 photon count detection, which should be considered. Therefore, we will design a high-speed photon-counting readout circuit in future studies.

Our indirect PDC system was developed for multi-energy imaging. However, a ^{137}Cs source was used to emit a single-energy gamma ray of 662 keV in this study. Therefore, multiple energy bin settings were not considered when acquiring the phantom images. Multi-energy imaging can be applied to radiation with a wide energy range, such as X-rays. By setting the energy bins, it is possible to accurately determine the linear attenuation coefficient information for energy. Thereby, the indirect PCD system can help K-edge imaging. K-edge images represent specific information of a certain material. In addition, multi-energy images could be acquired simultaneously with a single shot. Also, beam-hardening artifact could be reduced by using energy selective windows.

4. Conclusions

The present work demonstrates the potential of an indirect PCD system for 2D imaging. The results of this study show that it is possible to carry out indirect photon-counting imaging in electromagnetic transmission imaging. Future work will include an indirect PCD for low-energy photon detection and multi-energy imaging.

Acknowledgment

This research was supported by the National Foundation of Korea (NRF) funded by the Ministry of Education, Science and Technology (2018R1C1B5085189).

References

[1] R. K. Swank, J. Appl. Phys. **44**, 4199 (1973).
[2] J. P. Schlomka, E. Roessl, R. Dorscheid et al., Phys. Med. Biol. **53**, 4031 (2008).
[3] C. Xu, M. Persson, C. Han et al., IEEE Trans. Nucl. Sci. **60**, 437 (2013).
[4] K. Taguchi, Radiol. Phys. Technol. **10**, 8 (2017).
[5] S. Leng, M. Bruesewitz, S. Tao et al., Radiographics **39**, 729 (2019).
[6] M. J. Willemink, M. Persson, A. Pourmorteza et al., Radiology **289**, 293 (2018).
[7] H. S. Kim, J. H. Ha, S. H. Park et al., Nucl. Instrum. Appl. Radia. Isot. **67**, 1463 (2009).
[8] C. H. Baek, H. Lee, and D. Kim, Int. J. Eng. Tech. **7**, 78 (2018).
[9] Z. Deng, Y. Deng, and G. Chen, Sensors **20**, 5820 (2020).
[10] S. Kaviani, N. Zeraatkar, S. Sajedi et al., Phys. Med. **32**, 889 (2016).